Fuzzy directional enlacement landscapes for the evaluation of complex spatial relations

Michaël Clément, Camille Kurtz, Laurent Wendling

Fuzzy Directional Enlacement Landscapes for the Evaluation of Complex Spatial Relations

Michaël Clément[a,*], Camille Kurtz[b], Laurent Wendling[b]

[a] *Bordeaux INP, Univ. Bordeaux, CNRS, LaBRI UMR 5800, F-33400 Talence, France*
[b] *Université de Paris, LIPADE EA 2517, 75006 Paris, France*

Abstract

Structural spatial relations between image components are fundamental in the human perception of image similarity, and constitute a challenging topic in the domain of image analysis. By definition, some specific relations are ambiguous and difficult to formalize precisely by humans. In this work, we deal with the issue of evaluating complex spatial configurations, where objects can surround each other, potentially with multiple levels of depth. Based on a recently introduced spatial relation called enlacement, which generalizes the idea of surrounding for arbitrary objects, we propose a fuzzy landscape model that allows both to visualize and evaluate this relation directly in the image space, following different directions. Experiments on several characteristic examples highlight the interest and the behavior of this approach, allowing for rich interpretations of these complex spatial configurations.

Keywords: Evaluation of spatial relations, Fuzzy Directional Landscapes, Enlacement, Surrounding

1. Introduction

In recent years, there has been an increasing interest in using the spatial organization of objects in the field of image analysis. Characterizing such spatial relations is indeed a promising way to increase both the understanding and the accuracy of similarity perception between visual scenes or situations. Despite the fact that humans seem capable of apprehending spatial configurations with little to no efforts, in many cases it can be exceedingly difficult to quantitatively model these relations, mainly because they are highly prone to subjectivity. Standard all-or-nothing relations are clearly not suitable, and the interest of fuzzy relations was initially suggested by Freeman in the 70s [1] since they take imprecisions into account. Following this seminal work, numerous approaches were proposed for the analysis of spatial relations in various domains, ranging from shape recognition to computer vision [2]. These approaches provide interesting features that are able to describe efficiently most spatial relations (*i.e.*, metric, directional and topological relations).

Nevertheless, some specific spatial configurations remain difficult to describe without ambiguities. In particular, a challenging case is when objects of arbitrary shape are surrounding each other in complex patterns. Indeed, when objects exhibit multiple levels of depth (*i.e.*, spirals or spiky patterns) or are constituted of multiple connected components, using only the surrounding relation might not be sufficient to effectively model the spatial configuration. As an illustrative example, let us refer to the intuitive situations presented in Fig. 1. In these cases, we might be interested in modeling the region of space that is being surrounded by ghosts (reference object A). By answering such questions, it then becomes possible to quantify to which degree the character Mario (target object B) is surrounded, depending both on its shape and relative position to A. However, most existing models for the surrounding relation fall short at properly capturing the multiple components, the thickness, and the levels of depth of the reference object A, sometimes yielding counter-intuitive results.

To better formalize these complex spatial configurations, a new spatial relation called "*enlacement*"

*Corresponding author
Email address: michael.clement@labri.fr (Michaël Clément)

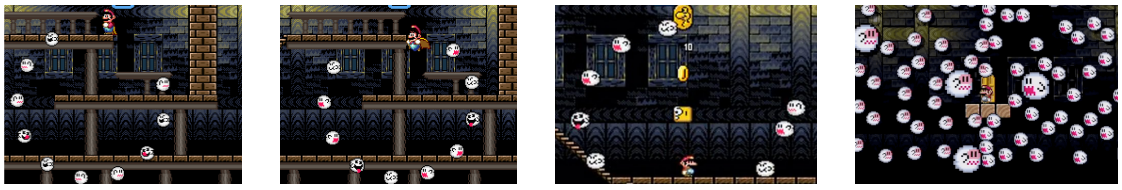

(a) (b) (c) (d)

Figure 1: Illustrative examples of spatial configurations where ghosts (reference object A) are *enlacing* the character Mario (target object B) to different degrees.

was recently introduced in [3]. In this work, the latter is defined as a generalization of spatial configurations where an arbitrary, potentially complex object surrounds or squeezes another object. Intuitively, an object is enlaced if it is unable to move from its initial location to a new one (in a particular direction) without having to cross the other object, taking into account its thickness and/or its levels of depth. For example, this allows to distinguish situations where an object would be enlaced by a thick rope or by a very thin sewing string. It is established as a relative concept, in the sense that it is always assessed for an object with regards to another. Also note that the relation is not symmetric: an object can be enlaced by another, but the opposite might not hold. From this definition, the more basic surrounding relation can be seen as a particular case of the enlacement relation: an object is surrounded if it is enlaced in all directions. Following the same intuition, the "*interlacement*" relation is further defined as a mutual enlacement of two objects (for example with two U-shapes or spirals imbricating each other).

The goal of this article – which is an extended version of [4] – is to propose an alternative method to quantify and evaluate these recently formalized spatial relations. Here, we seek to model the enlacement locally in the image, by quantifying to which degree each point in space is enlaced by an object. To this end, the rest of this article is organized as follows. In Section 2, we review related works to our approach, providing a more thorough background on the modeling of spatial relations for image analysis, and we further detail our contributions. Section 3 then recalls the model of [3] to build enlacement and interlacement descriptors. Based on the latter, and inspired by the works of Bloch on fuzzy landscapes [5], we present in Section 4 a generic model that allows to evaluate and visualize enlacement configurations from a local point of view and with directional granularity. Section 5 presents experimental results on different example tasks, showing the behavior and the interest of this model. In Section 6, we conclude and discuss some perspectives of this work.

2. Related Work

In the domain of spatial relations, two major research axes can usually be distinguished in the literature, based on two dual concepts [6]: the concept of *spatial relationship* and that of *relative position*.

On the one hand, it is possible to formulate a fuzzy evaluation of a spatial relation (for example "*to the left of*") for two objects, in order to describe their relative position. The fuzzy landscape model is a widely used method for providing these types of assessments [5]. This approach relies on the fuzzy modeling of a given spatial relation, directly in the image space, using morphological operators. From these landscapes, fuzzy measures such as the necessity-possibility intervals [7] can be used to evaluate the relation for different target objects. Typical applications include for example graph-based face recognition [8], brain segmentation from MRI [9], or handwritten text recognition [10].

On the other hand, the location of an object with regards to another can be modeled by a quantitative representation, in the form of a relative position descriptor. Different spatial relations can be assessed from this representation and the associated descriptors can be integrated in pattern recognition systems to match similar spatial configurations. Among the various relative position descriptors, the histograms of angles [11] and the histograms of forces [12] are widely used due to their ability to process pairwise information following a set of directions. They have a known behavior with regards to affine transformations [13], and efficient algorithms have been designed for their computation [14]. These descriptors are applied in differ-

ent works, such as the linguistic description of spatial relations [15], scene matching [16] or image retrieval [17, 18].

To summarize, fuzzy landscapes consist in determining the region of space matching a specific spatial relation, and relative position descriptors consist in characterizing the position of an object with regards to another, by combining different spatial features into a whole descriptor. However, although these two types of approaches allow interpretation of most typical spatial relations between objects, they usually cannot properly describe more complex configurations. In particular, many ambiguities arise when the objects are concave and/or composed of multiple connected components [19]. Consequently, several dedicated methods were proposed, focusing on more specific complex spatial relationships.

The "*surrounded by*" relation was first studied by Rosenfeld [20] and deepened by Vanegas [21] with a dedicated approach based on fuzzy landscapes. This relation has also been studied from the point of view of relative position descriptors, using an *ad hoc* method based on force histograms [22]. However, both of these approaches present some shortcomings: the former does not explicitly take into account the thickness of the objects (*i.e.*, it considers only the boundaries of the objects), while the latter suffers from what is called the "semantic inverse" problem (*i.e.*, it cannot properly distinguish if A surrounds B or the opposite). Another specific spatial relation is "*between*". This relation has been studied in detail in [19], involving definitions based on convex hulls and specific morphological operators. Applications of this spatial configuration for the analysis of histological images have been proposed by [23]. Other works have also been done on the spatial relation "*along*" [24], or to characterize the "*alignment*" and "*parallelism*" of objects in satellite images [25].

More recently, the ϕ-descriptor [26, 27] was introduced, which provides a generic framework to assess any spatial relation from a set of specific operators, notably inspired by Allen intervals [28]. This descriptor provides an important advancement, while requiring an extraction of a set of suitable operators dedicated to each usual spatial relation. It can detect whether if two objects are enlaced, but it is not directly able to quantify the importance of such a relationship (*i.e.*, it cannot measure how many times parts of an object are among parts of another), as it would require another level of integration.

In this context, recent works [3, 29] introduced both enlacement and interlacement descriptors, from the relative position point of view, in order to obtain a robust modeling of these relations for 2D objects. Based on this model, we propose to tackle the dual point of view, by considering fuzzy enlacement landscapes instead of enlacement descriptors. Initially introduced in [4], the goal of fuzzy enlacement landscapes is to visualize and evaluate these spatial configurations directly in the image space. Notably, it allows to highlight the local concavities of an object according to different directions. Inspired by these ideas, [30] also proposed a method based on quadrants to measure local concavities, but the approach is global and cannot take different directions into account. In the present article, our objective is to more thoroughly describe the fuzzy enlacement model, in particular by putting an emphasis on the geometrical properties of these fuzzy landscapes. Furthermore, we propose extended experimental validations, demonstrating the interest of this approach to characterize enlacement and surrounding configurations in various cases.

3. Directional Enlacement Model

The directional enlacement model was initially introduced in [3], mostly from the point of view of the relative position descriptors. In this section, we briefly recall the main definitions and principles of this model, which constitute the basis of our proposed approach.

3.1. Definitions

Two-Dimensional Objects. We define a 2D object A as a nonempty, bounded set of points, *i.e.*, $A \subset \mathbb{R}^2$. Equivalently, A can be defined by its characteristic (membership) function $\mathbb{1}_A : \mathbb{R}^2 \to \{0, 1\}$, which associates a binary value to each point $(x, y) \in \mathbb{R}^2$. This definition can easily be extended to the fuzzy case, where A is then defined as a fuzzy subset represented by its membership function $\mu_A : \mathbb{R}^2 \to [0, 1]$. More generally, it is also possible to interpret 2D objects as functions of compact support from $\mathbb{R}^2$ to $\mathbb{R}$, allowing for a more analytical manipulation, *i.e.*, A is defined by its representative function $f_A : \mathbb{R}^2 \to \mathbb{R}$.

Longitudinal Cuts. For ease of notation, throughout the rest of the article, the Euclidean plane $\mathbb{R}^2$

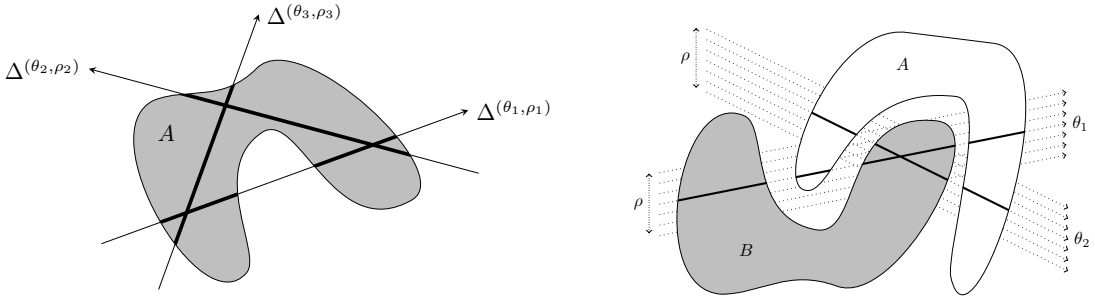

(a) Longitudinal cuts

(b) Parallel lines in different directions

Figure 2: Illustrative examples of the definitions used in the directional enlacement model [3].

and the complex plane $\mathbb{C}$ are equivalently identified by the isomorphism $(x, y) \in \mathbb{R}^2 \mapsto (x + iy) \in \mathbb{C}$.

Let $\theta \in \mathbb{R}$ be an orientation angle, and $\rho \in \mathbb{R}$ a distance from the origin. We define the oriented line of angle θ at the altitude ρ by the following set:

$$\Delta^{(\theta,\rho)} = \{e^{i\theta}(t + i\rho), t \in \mathbb{R}\}, \tag{1}$$

where $t \in \mathbb{R}$ denotes the coordinate of a point relatively to the line $\Delta^{(\theta,\rho)}$. Let $\Delta^{(\theta,\rho)}$ be such an oriented line, and A be an object. The subset $A \cap \Delta^{(\theta,\rho)}$ represents a one-dimensional slice of A, also called a *longitudinal cut*. In the case of binary objects, such a cut is either empty (the line does not intersect with the object) or composed of a finite number of segments, as illustrated in Fig. 2(a). In the continuous case, similarly to the functional notation of objects defined previously, a longitudinal cut of A along the line $\Delta^{(\theta,\rho)}$ can be formalized as a function $f_A^{(\theta,\rho)}$ such that:

$$\begin{array}{rccl} f_A^{(\theta,\rho)}: & \mathbb{R} & \longrightarrow & \mathbb{R} \\ & t & \longmapsto & f_A(e^{i\theta}(t + i\rho)), \end{array} \tag{2}$$

where t represents the 1D coordinate of a point along the line $\Delta^{(\theta,\rho)}$ and $f_A^{(\theta,\rho)}(t)$ is the representative value of this point on the plane, according to object A.

3.2. Enlacement Model

Let (A, B) be a couple of objects. The goal is to describe how A is enlaced by B. The intuition is to capture the occurrences of points of A being *between* points of B. To determine such occurrences, objects are handled in a one-dimensional case, using longitudinal cuts along oriented lines. For a given oriented line $\Delta^{(\theta,\rho)}$, the idea is to combine the quantity of object A (represented by $f_A^{(\theta,\rho)}$) located simultaneously *before* and *after* object B (represented by $f_B^{(\theta,\rho)}$). Let f and g be two bounded measurable functions with compact support from $\mathbb{R}$ to $\mathbb{R}$. The enlacement of f with regards to g is defined as:

$$E(f, g) = \int_{\mathbb{R}} g(x) \int_x^{+\infty} f(y) \int_y^{+\infty} g(z)\, \mathrm{d}z\, \mathrm{d}y\, \mathrm{d}x. \tag{3}$$

The scalar value $E(f_A^{(\theta,\rho)}, f_B^{(\theta,\rho)})$ represents the enlacement of A by B along the oriented line $\Delta^{(\theta,\rho)}$. For binary objects, it corresponds to the total number of ordered triplets of points on the oriented line, which can be seen as arguments to put in favor of the proposition *"A is enlaced by B"* in the direction θ. More details about algorithmical considerations can be found in [3].

The set of parallel lines $\{\Delta^{(\theta,\rho)}, \rho \in \mathbb{R}\}$ in direction θ slices the objects into sets of longitudinal cut functions (see Fig. 2(b)). To measure the global enlacement of A with regards to B in direction θ, we aggregate the one-dimensional enlacement values obtained for each of these longitudinal cuts. The enlacement of A by B in direction θ is therefore defined by:

$$\mathcal{E}_{AB}(\theta) = \frac{1}{\|A\|_1 \|B\|_1} \int_{-\infty}^{+\infty} E(f_A^{(\theta,\rho)}, f_B^{(\theta,\rho)})\, \mathrm{d}\rho, \tag{4}$$

where $\|A\|_1$ and $\|B\|_1$ denote the areas of A and B. This normalization results in scale invariance [3]. In the binary case, this definition corresponds to a number of triplets of points to put in favor of *"A is enlaced by B"* along the longitudinal cuts in this direction. Intuitively, it can be interpreted as the quantity of B traversed while sliding the object A in the direction θ, but also with regards to the quantity of B located on the opposite direction.

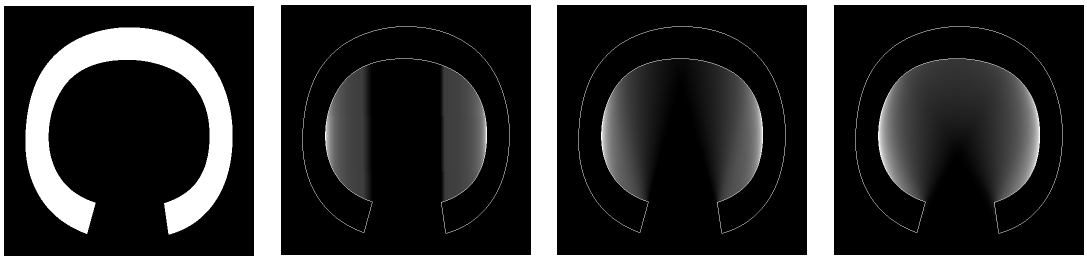

(a) Object A (b) $\mu_{\mathcal{E}}^{A}(\frac{\pi}{2}, 0)$ (c) $\mu_{\mathcal{E}}^{A}(\frac{\pi}{2}, \frac{\pi}{6})$ (d) $\mu_{\mathcal{E}}^{A}(\frac{\pi}{2}, \frac{\pi}{3})$

Figure 3: *Fuzz-DEL*s of a binary object A, for fixed direction θ and increasing width ω. In (b, c and d), A is outlined in white.

In [3], this model was considered from the point of view of the relative position descriptors, by building an enlacement histogram $\mathcal{E}_{AB}$, which characterizes how A is enlaced by B in different directions. In the next section, we propose to adapt this model from a local evaluation point of view, using a fuzzy approach that allows to represent enlacement configurations directly in the image space.

4. Fuzzy Enlacement Landscapes

We present here how to extend the directional enlacement model to evaluate the enlacement of objects in the image space from a local point of view, inspired by the works of Bloch [5] on fuzzy landscapes for classical spatial relations.

4.1. Definition

A fuzzy enlacement landscape of an object A should be a representation of the region of space that is enlaced by A. The initial enlacement model being essentially directional, we propose to follow the same philosophy and to define directional enlacement landscapes. Let A be a binary object (*i.e.*, represented here as $f_A : \mathbb{R}^2 \to \{0, 1\}$). In a given direction θ, for a point outside of A located at (ρ, t) coordinates in the rotated frame, its local enlacement value can be defined as the quantity of object A located simultaneously *before* and *after* the point along the considered oriented line. This principle can be formalized by the following product of two integrals:

$$\mathcal{E}_A(\theta)(\rho, t) = \frac{1}{\|A\|_1} \int_t^{+\infty} f_A^{(\theta,\rho)}(x)\,\mathrm{d}x \int_{-\infty}^{t} f_A^{(\theta,\rho)}(x)\,\mathrm{d}x. \tag{5}$$

When applied for all (ρ, t) coordinates, $\mathcal{E}_A(\theta)$ can actually be seen as a 2D landscape representing the local enlacement values of the points outside of the object A. This image can be normalized into the $[0, 1]$ range of values in order to be interpreted as a fuzzy set, which we call a *Fuzzy Directional Enlacement Landscape* (*Fuzz-DEL*). It can be defined by the following functional:

$$\begin{array}{rccc} \mu_{\mathcal{E}}^{A}: & \mathbb{R} & \longrightarrow & (\mathbb{R}^2 \longrightarrow \mathbb{R}) \\ & \theta & \longmapsto & (\rho, t) \in \mathbb{R}^2 \longmapsto \mu_{\mathcal{E}}^{A}(\theta)(\rho, t), \end{array} \tag{6}$$

where we have

$$\mu_{\mathcal{E}}^{A}(\theta)(\rho, t) = \frac{\mathcal{E}_A(\theta)(\rho, t)}{\max\limits_{\rho,t} \mathcal{E}_A(\theta)(\rho, t)}. \tag{7}$$

The goal of such a landscape is to assess and visualize to which degree each point is enlaced by the object A in a fixed direction θ. It is interesting to note that the non-zero values of this landscape are necessarily located inside the object's concavities. This is particularly interesting from an algorithmic point of view, since it allows restriction of the computation to points located in the convex hull of A (and outside of A).

As the definition of $\mu_{\mathcal{E}}^{A}(\theta)$ is focused on a single direction, we also propose to aggregate fuzzy landscapes across multiple orientation angles. Let $\theta \in [0, \pi]$ be an orientation angle and $\omega \in [0, \pi]$ a width parameter. The *Fuzz-DEL* on the interval $[\theta - \frac{\omega}{2}, \theta + \frac{\omega}{2}]$ is defined as follows:

$$\mu_{\mathcal{E}}^{A}(\theta, \omega)(\rho, t) = \frac{1}{\omega} \int_{\theta-\frac{\omega}{2}}^{\theta+\frac{\omega}{2}} \mu_{\mathcal{E}}^{A}(\alpha)(\rho, t)\,\mathrm{d}\alpha, \tag{8}$$

where θ represents the direction on which the fuzzy landscape is focused, while ω controls the width of the interval, allowing to measure either a narrow direction or a more global one. In particular, the landscape that aggregates all directions is denoted by $\widetilde{\mu}_{\mathcal{E}}^{A} = \mu_{\mathcal{E}}^{A}(\frac{\pi}{2}, \pi)$.

In order to illustrate these definitions, Fig. 3 and 4 show the *Fuzz-DEL*s obtained for two different objects. On the one hand, Fig. 3 illustrates the

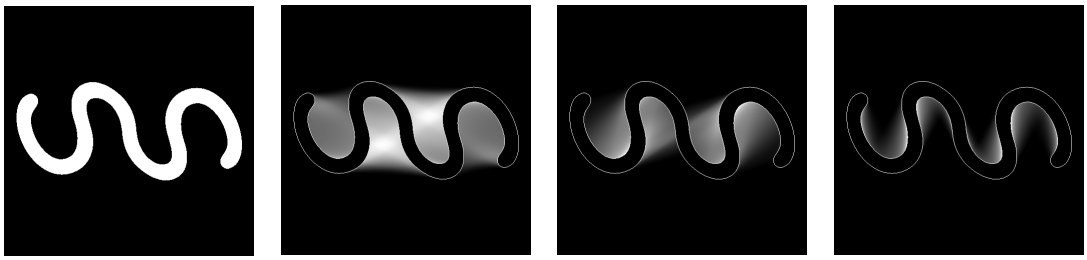

(a) Object A (b) $\mu_{\mathcal{E}}^{A}(0, \frac{\pi}{3})$ (c) $\mu_{\mathcal{E}}^{A}(\frac{\pi}{4}, \frac{\pi}{3})$ (d) $\mu_{\mathcal{E}}^{A}(\frac{\pi}{2}, \frac{\pi}{3})$

Figure 4: *Fuzz-DEL*s of a binary object A, for fixed width ω and different directions θ. In (b, c and d), A is outlined in white.

impact of the width parameter ω for a fixed vertical direction ($\theta = \frac{\pi}{2}$). Note that the landscape would be identical for the opposite direction ($\theta = \frac{3\pi}{2}$) because of symmetry (this is notably checked in the next section discussing geometrical properties). For $\omega = 0$, zero-valued points are found in the center of the object, showing that these points are not enlaced vertically by A. Intuitively, if another object was located here, it would be able to move in the vertical direction without crossing A (*i.e.*, the object could slide downwards). We also observe that when ω increases, the fuzzy landscape progressively gets smoother, taking into account a wider range of directions. On the other hand, Fig. 4 shows enlacement landscapes on another object for different directions θ (with a fixed width $\omega = \frac{\pi}{3}$). From these examples, we can see that *Fuzz-DEL*s are able to capture directional concavities. Most notably, in the horizontal direction ($\theta = 0$), the local enlacement is relatively high, and the values are higher the deeper we get inside the shape. In the vertical direction ($\theta = \frac{\pi}{2}$), the *Fuzz-DEL* is mostly empty, except for some small concavities.

4.2. Geometrical Properties

Here, we enumerate some mathematical properties of the proposed fuzzy enlacement landscapes with regards to some geometric transformations. The proofs for these properties are provided in Appendix A.

Property 1 (Translation). *A translation of an object A also translates the corresponding enlacement landscapes. Let $T_{\mathbf{v}}$ be a translation by vector $\mathbf{v} = [v_\rho, v_t] \in \mathbb{R}^2$. For any $(\rho, t) \in \mathbb{R}^2$, we have:*

$$\mu_{\mathcal{E}}^{T_v(A)}(\theta)(\rho, t) = \mu_{\mathcal{E}}^{A}(\theta)(\rho - v_\rho, t - v_t). \quad (9)$$

Property 2 (Rotation). *A rotation of an object A also rotates the corresponding enlacement landscapes. Let R_α be a rotation of angle $\alpha \in \mathbb{R}$. For any $(\rho, t) \in \mathbb{R}^2$, we have:*

$$\mu_{\mathcal{E}}^{R_\alpha(A)}(\theta)(\rho, t) = \mu_{\mathcal{E}}^{A}(\theta - \alpha)(\rho, t). \quad (10)$$

Property 3 (Periodicity). *For an object A, enlacement landscapes are symmetric, with period π. For all $\theta \in \mathbb{R}$, we have:*

$$\mu_{\mathcal{E}}^{A}(\theta + \pi) = \mu_{\mathcal{E}}^{A}(\theta). \quad (11)$$

Property 4 (Scaling). *A scaling of an object A also scales the corresponding enlacement landscapes by the same scaling factor. Let S_λ be a scaling of factor $\lambda \in \mathbb{R}$. For any $(\rho, t) \in \mathbb{R}^2$, we have:*

$$\mu_{\mathcal{E}}^{S_\lambda(A)}(\theta)(\rho, t) = \mu_{\mathcal{E}}^{A}(\theta)(\lambda\rho, \lambda t). \quad (12)$$

Note that these properties extend naturally for *Fuzz-DEL*s with a width parameter ω. Moreover, some of these properties (*i.e.*, rotation and scaling) are also verified experimentally in Section 5.2.

4.3. Algorithmic Considerations

The definitions of *Fuzz-DEL*s have been introduced theoretically in the continuous domain, using analytical notations to manipulate 2D objects as 1D cuts. In this section, we discuss the practical implementation of our approach for discrete, binary objects defined on a classical pixel grid. A naive Python implementation of this algorithm has been made available online[1], allowing for the computation of *Fuzz-DEL*s for binary objects in different directions.

For the sake of simplicity, we consider discrete square images composed of N pixels (*i.e.*, images of size $\sqrt{N} \times \sqrt{N}$), where an object corresponds to a set of binary pixels. Note that these object pixels do not have to be spatially connected, allowing

[1] `https://github.com/clememic/enlacement`

for objects made up of multiple components. For a given object A, the *Fuzz-DEL* $\mu^A_{\mathcal{E}}(\theta)$ in direction θ can be mapped to a gray-valued image of the same size. To compute the values of this image, we first generate all the discrete parallel lines in direction θ of the image (Equation 1). An initial line of sufficient length is built using the classical Bresenham line-drawing algorithm. This line is then shifted to obtain all the parallel lines, ensuring that each pixel is counted once and only once. From these lines, we consider the longitudinal cuts of A (segments crossing the object), as well as the cuts of its complement $\bar{A}$ in the image support (segments crossing the background). We then assign to the segments of $\bar{A}$, the cumulated product of segments of A that are simultaneously before and after (Equation 5); if there is no such case, the whole segment is assigned to zero values. The segment lengths are computed in an isotropic manner, taking into account the orientation angle (*i.e.*, the number of pixels in a segment is normalized by the sine/cosine depending on the quadrant). This allows to mitigate some discretization issues due to the square nature of the pixel grid. Note that more advanced strategies regarding these discrete aspects could be considered, such as in the works of [31] for example.

In terms of complexity, the number of points on a line is in $\mathcal{O}(\sqrt{N})$, and the lookup for segments results in a cubic complexity (*i.e.*, for each segment in $\bar{A}$, we need to enumerate segments of A before and after), inducing a worst-case complexity in $\mathcal{O}(N\sqrt{N})$. The number of parallel lines in the image is bounded by $\sqrt{N}$. In the end, the computation of the *Fuzz-DEL* $\mu^A_{\mathcal{E}}(\theta)$ in a direction θ has an upper bound worst-case complexity of $\mathcal{O}(N^2)$ where N is the number of pixels in the image. Note that this complexity is not achieved in practice, as it would correspond to a highly distorted object, for example following a checkerboard pattern. The actual complexity is relative to the number of cuts in each parallel line, which depends on the shape of the considered object.

4.4. Fuzzy Evaluations

In the previous definitions, a reference object A is considered, and different *Fuzz-DEL*s can be derived from it. These fuzzy landscapes allow to visualize the enlacement that A exerts around itself. In the following, we show how to further exploit these landscapes to evaluate the degree to which a target object B is enlaced by A, using classical fuzzy operators such as necessity and possibility. Indeed, several works on spatial relations have used measures based on fuzzy sets to evaluate their approaches [8, 9, 10] (the reader can also refer to [32] for a summary of classical fuzzy measures). Let μ_A and μ_B be two fuzzy sets over $\mathbb{R}^2$. To evaluate how μ_B matches with μ_A, the necessity N and possibility Π are respectively defined as follows:

$$\Pi(\mu_A, \mu_B) = \sup_{x,y} t(\mu_A(x,y), \mu_B(x,y)), \tag{13}$$

$$N(\mu_A, \mu_B) = \inf_{x,y} T(\mu_A(x,y), 1 - \mu_B(x,y)), \tag{14}$$

where t is a fuzzy intersection (t-norm) and T is a fuzzy union (t-conorm). In this work, the min and max operators are chosen for t-norm and t-conorm respectively, but other fuzzy operators could be considered. The mean value is also commonly used:

$$M(\mu_A, \mu_B) = \frac{\sum_{x,y} t(\mu_A(x,y), \mu_B(x,y))}{\sum_{x,y} \mu_A(x,y)} \tag{15}$$

In our context, these fuzzy measures can be applied to evaluate how a target object B (represented by its membership function μ_B) matches with a *Fuzz-DEL* $\mu^A_{\mathcal{E}}(\theta, \omega)$ of a reference object A. The necessity-possibility interval $[N(\mu^A_{\mathcal{E}}(\theta,\omega), \mu_B), \Pi(\mu^A_{\mathcal{E}}(\theta,\omega), \mu_B)]$ is a fuzzy evaluation of how B is enlaced by A in direction θ, with the necessity being a pessimist point of view (*i.e.*, the evaluation cannot be larger than the minimum value), while the possibility represents a more optimistic point of view (by using the maximum value). For example, this interval allows to nuance the interpretation depending on the thickness of the reference object: the possibility will be 1 as long as the object is enlaced by a 1-pixel thin border, but the necessity could be lower if the thickness is not homogeneous relative to its area.

The geometrical properties of *Fuzz-DEL*s presented in Section 4.2 naturally induce some properties on these evaluations. Because they are overall measures on the fuzzy landscapes (*i.e.*, minimum, maximum and mean values), it follows that they are invariant with regards to translations and scalings of the objects (because of area normalization), and that rotations result in circular shifts of the evaluations equivalent to the rotation angle. This evaluation strategy will be further studied in the upcoming experiments.

5. Experimental Results

In this section, we report experimental results on different illustrative examples to highlight the in-

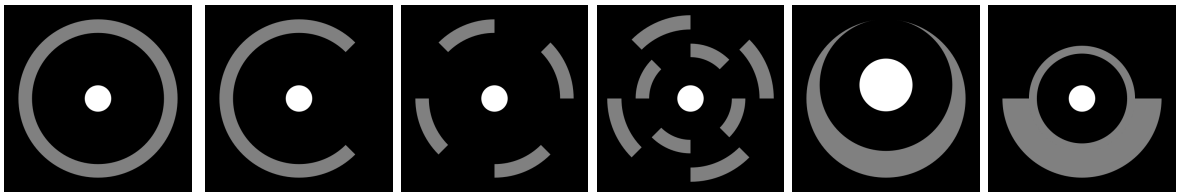

(a) (b) (c) (d) (e) (f)

Figure 5: Examples of typical surrounding configurations (gray: reference object A; white: target object B).

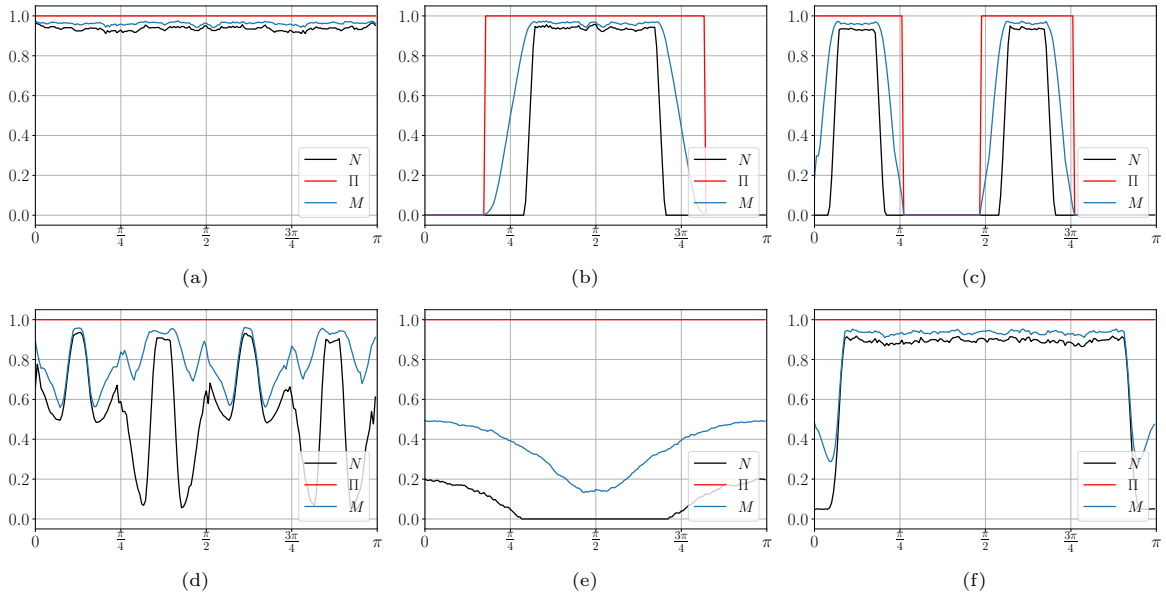

(a) (b) (c) (d) (e) (f)

Figure 6: Directional necessity, possibility and mean profiles measuring the surrounding configurations of Fig. 5.

terest and the behavior of our model. These experiments are organized around two main applications. The first one is to evaluate the specific relation *"surrounded by"* on typical configurations (Section 5.1). As mentioned previously, this relation can be considered as a particular case that can be derived from the directional enlacement model. We also present a robustness study highlighting the geometrical properties of the fuzzy enlacement landscapes with regards to these configurations (Section 5.2). The second application is to evaluate the spatial relation *"enlaced by"* in a more generic sense (Section 5.3), in particular when the reference objects have multiple degrees of concavities. To this end, we first illustrate the model on an illustrative example, then we propose a more thorough experiment on the MPEG7 shape dataset. Finally, we also propose some preliminary results on the prospective concept of *interlacement* landscapes (Section 5.4).

5.1. Surrounding relation

The *"surrounded by"* relation is easily apprehended by human perception, but is particularly challenging to evaluate quantitatively. It is usually modeled by the "all directions" point of view, *i.e.*, an object surrounds another object if it is located in all directions. In the following, we adopt the same insight, but we adapt it to the enlacement model: an object is surrounded if it is enlaced by the other object in all directions.

Fig. 5 presents characteristic examples of surrounding configurations that we assessed using our fuzzy evaluation strategy. In each image, the reference object A is in gray and the target object B is the white circle at the image center.

For this application, we propose a specific way to evaluate the surrounding relation using our enlacement landscapes. The target object B is projected into a *Fuzz-DEL* $\mu_{\mathcal{E}}^{A}(\theta, \omega)$, and normalized as

Table 1: surrounding evaluations (necessity-possibility intervals and mean values) obtained for the configurations (a) to (f) of Fig. 5. For the approach of [22], only mean values are available.

	Matsakis *et al.* [22]	Vanegas *et al.* [21]	Enlacement $\mathcal{E}_{AB}$ [3]	$[N_{\mathcal{S}}^{AB}, \Pi_{\mathcal{S}}^{AB}]$, $M_{\mathcal{S}}^{AB}$
(a)	0.99	[1.00, 1.00], 1.00	[1.00, 1.00], 1.00	[0.94, 1.00], 0.96
(b)	0.50	[0.70, 0.79], 0.76	[0.50, 0.63], 0.55	[0.36, 0.64], 0.48
(c)	0.74	[0.50, 0.54], 0.52	[0.40, 0.49], 0.45	[0.25, 0.53], 0.39
(d)	0.94	[0.93, 1.00], 0.97	[0.75, 1.00], 0.95	[0.54, 1.00], 0.79
(e)	0.16	[0.76, 0.90], 0.85	[0.52, 1.00], 0.73	[0.07, 1.00], 0.36
(f)	0.25	[0.94, 1.00], 0.99	[0.48, 1.00], 0.82	[0.77, 1.00], 0.85

a fuzzy set by the following:

$$\mu_{\mathcal{E}}^{AB}(\theta,\omega) = \frac{\min\limits_{\rho,t}\left(\mu_{\mathcal{E}}^{A}(\theta,\omega)(\rho,t), \mu_B(\rho,t)\right)}{\max\limits_{\rho,t}\mu_{\mathcal{E}}^{A}(\theta,\omega)(\rho,t)}. \quad (16)$$

Then, the necessity $N(\mu_{\mathcal{E}}^{AB}(\theta,\omega), \mu_B)$ and possibility $\Pi(\mu_{\mathcal{E}}^{AB}(\theta,\omega), \mu_B)$ evaluations are obtained for different values of $\theta \in [0,\pi]$. This results in informative directional necessity and possibility profiles, which can be further exploited to derive global evaluations of how B is surrounded by A. Such evaluations can be obtained by averaging the profiles over all directions:

$$N_{\mathcal{S}}^{AB} = \frac{1}{\pi}\int_0^{\pi} N(\mu_{\mathcal{E}}^{AB}(\theta,\omega), \mu_B)\,\mathrm{d}\theta, \quad (17)$$

$$\Pi_{\mathcal{S}}^{AB} = \frac{1}{\pi}\int_0^{\pi} \Pi(\mu_{\mathcal{E}}^{AB}(\theta,\omega), \mu_B)\,\mathrm{d}\theta, \quad (18)$$

$$M_{\mathcal{S}}^{AB} = \frac{1}{\pi}\int_0^{\pi} M(\mu_{\mathcal{E}}^{AB}(\theta,\omega), \mu_B)\,\mathrm{d}\theta. \quad (19)$$

In practice, these are derived by averaging over a finite set of discrete directions in $[0,\pi]$. In these experiments, the number of discrete directions was fixed to $k = 180$. Moreover, we fixed ω to a low value of $\frac{\pi}{36}$ (5 degrees) to take into account different directions individually, while smoothing out some discretization issues. These evaluations thus correspond to average necessities, possibilities and means over all directions.

Fig. 6 shows the directional necessity and possibility profiles obtained for the six configurations of Fig. 5. To complement these results, Table 1 also presents the average surrounding necessity-possibility intervals $[N_{\mathcal{S}}^{AB}, \Pi_{\mathcal{S}}^{AB}]$, obtained from the previous directional profiles, to quantitatively evaluate the global surrounding of the target objects for these configurations. For comparison purposes, we also present the results of the related approach proposed by Matsakis *et al.* [22], which is based on the force histogram between the objects, but cannot distinguish which object surrounds the other. We also report the results from the approach of Vanegas *et al.* [21] which is also based on a fuzzy landscape framework, dedicated to the surrounding relation by considering only the visible concavities of the reference object. Note that this approach does not explicitly take into account the thickness of the objects, thus potentially explaining the main differences in the evaluations. The results obtained by [3] with the initial enlacement descriptors are also reported in this comparative study.

Considering the fact that surrounding evaluations are highly subjective, our goal here is not to argue that an approach is better than another, but to illustrate that the proposed *Fuzz-DEL*s can provide a pertinent evaluation and novel point of view regarding this surrounding spatial relation. In this context, we briefly discuss the results of each configuration, highlighting the main differences with the comparative approaches:

- In situation (a), the object is completely surrounded. Both our necessity and possibility evaluations agree that the reference object A is surrounded in all directions. The pessimistic point of view is not always equal to 1 due to some discretization issues at the pixel level. The other approaches also provide similar evaluations. However, note that if we evaluate the opposite scenario (*i.e.*, if we exchange A and B), the approach of [22] still gives 0.99, which is counter-intuitive, while our approach gives evaluations of 0, as expected. This observation is also true for the following examples;
- In configuration (b), the object is only partially surrounded. Both our pessimistic and optimistic profiles agree that the reference object A is surrounded in the vertical directions, but not in the horizontal directions. The gradual transition of the configuration (notably captured

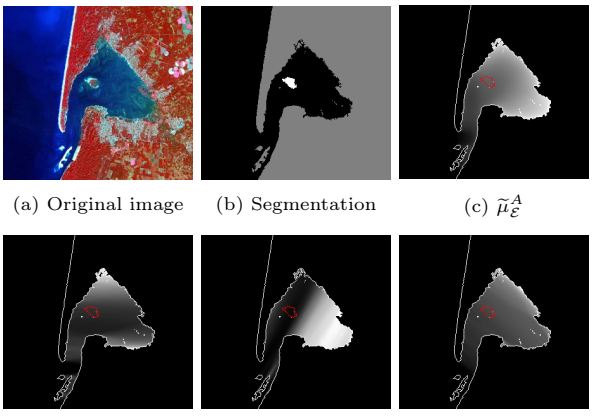

(a) Original image (b) Segmentation (c) $\widetilde{\mu}^A_{\mathcal{E}}$

(d) $\mu^A_{\mathcal{E}}(0, \frac{\pi}{6})$ (e) $\mu^A_{\mathcal{E}}(\frac{\pi}{3}, \frac{\pi}{12})$ (f) $\mu^A_{\mathcal{E}}(\frac{3\pi}{4}, \frac{\pi}{6})$

Figure 7: Applicative example of a real world surrounding configuration. The satellite image represents the *Bassin d'Arcachon* (France). (b) Object A is gray and object B is white. (c–f) A is outlined in white and B is outlined in red.

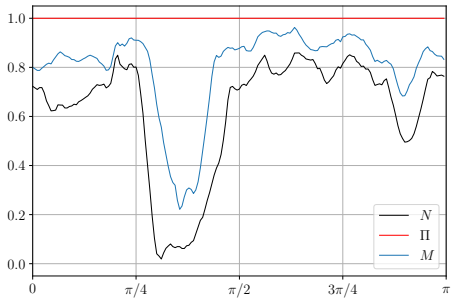

(a)

Matsakis *et al.* [22]	0.51
Vanegas *et al.* [21]	[0.68, 0.85], 0.79
Enlacement $\mathcal{E}_{AB}$ [3]	[0.35, 1.00], 0.62
$[N^{AB}_{\mathcal{S}}, \Pi^{AB}_{\mathcal{S}}]$, $M^{AB}_{\mathcal{S}}$	[0.63, 1.00], 0.80

(b)

Figure 8: Surrounding evaluations for the configuration depicted in Fig. 7. (a) Directional necessity, possibility and mean profiles. (b) Overall evaluations and comparison with related approaches, as in Table 1.

by the mean profile in blue) can be seen along the diagonal directions. Depending on the approaches, global evaluations in Table 1 can be a bit divergent but not counter-intuitive, with mean values ranging from 0.48 for our approach to 0.76 for [21];

- The object is also partially surrounded in situation (c), where about half of the surrounding circle has been cut out. We can observe the same kind of gradual transition in our profiles corresponding to the directions where the surrounding circle is cut. Again, global evaluations follow the intuition, ranging from 0.39 to 0.74 for mean values;

- In scenario (d), small parts were added preventing the object to leave without crossing the surrounding object, and therefore our optimistic profile is 1 for all directions, while the pessimist one oscillates but is never zero. Most comparative approaches tend to agree that that the object is surrounded to high degrees. Our approach provides a more moderate mean value of 0.79;

- Configuration (e) shows a reference object of varying thickness, that our approach is specifically designed to take into account. In this case, the possibility profile is always 1 (the target object is considered as surrounded), yet the necessity and mean profiles reveal that in the vertical directions, the object could escape by crossing a small portion of the reference object, and therefore surrounding evaluations are lower;

- Finally, these observations about thickness are reinforced in the situation (f), where the white object can not escape in any direction without crossing at least partially the gray object. Therefore, the possibility profile is 1 everywhere. However, because the reference object is thinner in its upper part, the necessity and mean profiles are lower in most directions, with an average of 0.85. Note that [22] gives a non-intuitive evaluation of 0.25, while the approach of [21] does not take the thickness into account, and therefore gives an evaluation of 0.99.

To show the potential of our approach on real data, we evaluated the *"surrounded by"* relation on geographical objects extracted from a satellite image (Fig. 7 (a)). This image[2] represents the *Bassin d'Arcachon* (France) and has been acquired by the FORMOSAT-2 satellite (with a spatial resolution of 8 meters) and four spectral bands (Near-Infrared, Red, Green and Blue). The image was segmented with the Mean-Shift algorithm to produce a 3-class image (Fig. 7 (b)) composed of an island (*i.e.*, *l'île*

[2]Thanks to the CNES agency and the Kalideos project (`http://kalideos.cnes.fr/`).

aux oiseaux, reference object A) enclosed into the bay and the land coast (target object B). For illustrative purposes, Fig. 7 (c–f) present the *Fuzz-DEL*s of the bay object for different directions θ and widths ω. In particular, (c) shows the overall landscape $\widetilde{\mu}^A_{\mathcal{E}}$ that aggregates all directions, and (e) shows the direction where the target object is the least enlaced (*i.e.*, for $\theta = \frac{\pi}{3}$). The corresponding directional necessity and possibility profiles are plotted in Fig. 8 (a), and the respective fuzzy surrounding evaluations $[N_{\mathcal{S}}^{AB}, \Pi_{\mathcal{S}}^{AB}]$ are reported in Fig. 8 (b) along with comparative methods. We can observe different mean surrounding evaluations for the different approaches. However, our possibility evaluation is 1.00, meaning that the target object cannot escape the area without crossing at least some parts of the reference object.

5.2. Robustness study

In this section, we propose to study the robustness of our approach to different types of transformations and alterations applied to the input objects. This study allows us to highlight the behavior of our evaluation model with regards to the geometrical properties (from Section 4.2) of our model in the context of the surrounding spatial relation.

5.2.1. Rotations

In order to check the quasi-invariance of enlacement landscapes with regards to rotations in the discrete domain, we applied global rotations to the images of Fig. 5, with no interpolation to preserve the binary nature of the configurations. Because of the directional nature of the enlacement landscapes, our hypothesis is that a rotation of the image should induce a circular shift in the resulting necessity-possibility profile.

This behavior is illustrated in Fig. 9, where three profiles are represented. To obtain these profiles, we performed three successive rotations (by setting the rotation angle θ to $\frac{\pi}{4}$, $\frac{\pi}{2}$ and π) of the image related to configuration (b) from Fig. 5. For each rotated image, we built the directional necessity and possibility profiles from the corresponding *Fuzz-DEL*s. As it was expected, the profiles obtained from the rotated images present homogeneous circular shifts where the shifting values are equal to the rotation angle θ of the image. Note that the rotation of π (Fig. 9(c)) also illustrates the π-periodicity property of our model (*i.e.*, same profiles as Fig. 6(b)). Naturally, the surrounding necessity-possibility intervals $[N_{\mathcal{S}}^{AB}, \Pi_{\mathcal{S}}^{AB}]$ related to these rotated images (reported in the captions of Fig. 9) are similar to line (b) of Table 1. Some slight differences can be observed and may be due to potential discretization issues when rotating the images without interpolation. Then, we applied this rotation protocol over 16 angles on the six proposed surrounding configurations, and we obtained an overall mean-squared error (MSE) in the order of 10^{-4} on average for the necessity-possibility and mean profiles compared to the reference ones manually shifted by the rotation angles.

Table 2: MSE obtained between the directional necessity-possibility and mean profiles from reference images of Fig. 5 and their downscaled versions (10 successive downscalings with linearly spaced factors in $[0, 1]$).

	$N_{\mathcal{S}}^{AB}$	$\Pi_{\mathcal{S}}^{AB}$	$M_{\mathcal{S}}^{AB}$
(a)	6.8e-04	0.0e+00	2.1e-04
(b)	2.5e-04	5.6e-03	9.7e-05
(c)	1.7e-04	1.9e-03	8.4e-05
(d)	9.4e-04	0.0e+00	2.5e-04
(e)	1.1e-04	0.0e+00	9.5e-05
(f)	8.3e-04	0.0e+00	2.7e-04

5.2.2. Scaling

In the same spirit, we propose to evaluate the robustness of *Fuzz-DEL*s with regards to the downscaling (*i.e.*, homothety transformations) of the images of Fig. 5. From these configurations, depicted by initial images of size 500×500, we applied 10 successive downscalings with linearly spaced factors in $[0, 1]$, resulting in images of sizes down to 31×31. For each of these downscalings, we computed the corresponding *Fuzz-DEL*s in all directions and generated the overall surrounding evaluations.

In Table 2, we report the average mean-squared errors (MSE) obtained between the directional necessity-possibility and mean profiles from the reference image and the downscaled ones. From these results, and similarly to the rotation experiments, we observe very small errors, of the order of 10^{-4} on average, highlighting the robustnesses of our approach to the downscaling and discretization of the studied objects. Notably, we can notice the very small error for the optimistic point of view on configurations (b) and (c), which correspond to the only two configurations where the possibility evaluations are not equal 1 in all directions (see Fig. 6 (b) and (c)) and therefore the downscalings of the images may introduce some small discontinuities. Such results seem to experimentally confirm that

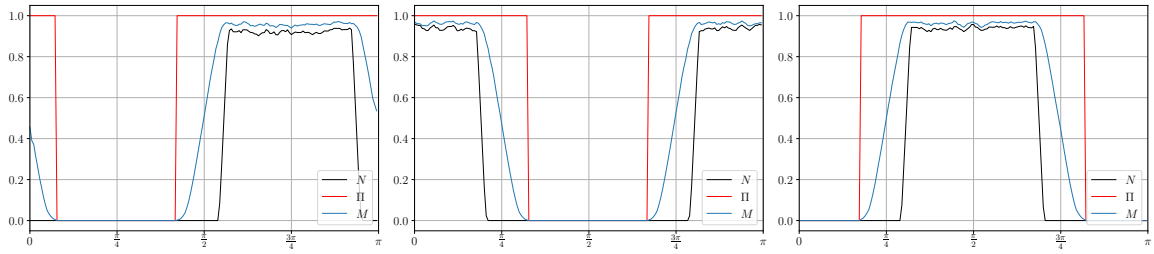

(a) $\theta = \frac{\pi}{4}$, $[0.35, 0.66], 0.48$ (b) $\theta = \frac{\pi}{2}$, $[0.36, 0.66], 0.48$ (c) $\theta = \pi$, $[0.36, 0.64], 0.48$

Figure 9: Behavior of surrounding profiles and evaluations with Fuzz-DELs for different rotations of the objects from the configuration (b) of Fig. 5.

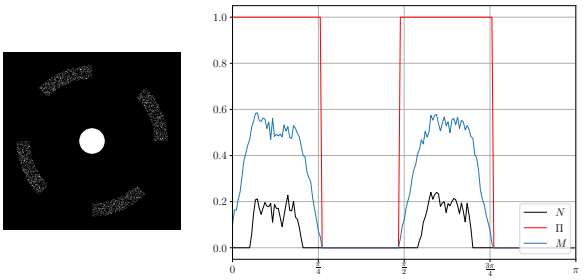

(a) Configuration (c), $[0.05, 0.53], 0.22$

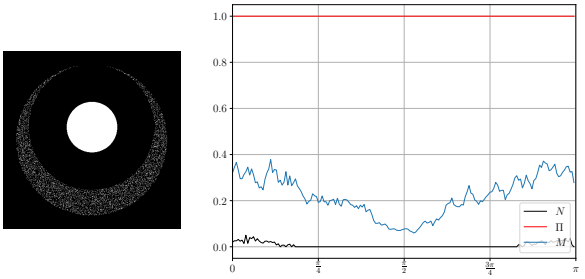

(b) Configuration (e), $[0.01, 1.00], 0.22$

Figure 10: Behavior of surrounding profiles and evaluations with *Fuzz-DELs* following the degradation of the reference object with Speckle noise (variance of $\sigma = 0.28$). The two examples correspond to the configurations (c) and (e) of Fig. 5.

our enlacement landscapes are invariant to scaling transformations, up to some negligible discretization issues.

5.2.3. Robustness to noise

Finally, we evaluated the behavior of *Fuzz-DELs* with regards to the application of artificial noise to the reference object. We gradually added Speckle noise, which is a multiplicative noise degrading the interior of the object, to the reference object prior to computing the corresponding *Fuzz-DELs* and surrounding evaluations. This kind of noise can have a strong impact on the behavior of the approach, as it can change the topology of the object by creating different cavities, holes and discontinuities.

In Fig. 10, we present some examples of obtained results for the surrounding configurations (c) and (e) from Fig. 5. These two examples correspond to a Speckle noise applied with a variance of $\sigma^2 = 0.28$. From these results, and by comparison to the results of Fig. 6 and Table 1, we can observe that the overall shapes of the necessity-possibility and mean profiles are preserved following the degradation of the reference object. The possibility profiles remain unchanged (since Speckle noise does not add pixels outside of the initial object), while the necessity values are lower, as Speckle noise may create small holes and cavities inside the object. By interpreting the enlacement as the surface area (*i.e.*, the amount of material) to be traversed to escape from the reference object in a given direction, this is the expected behavior when applying this kind of noise. These experiences strengthen us in our intuition that our approach for the evaluation of surrounding (and more generally enlacement) configurations can provide relevant evaluation results even in the case of noisy objects, a situation that can often occur, for example, if the objects have been extracted using segmentation algorithms.

5.3. Enlacement relation

To pursue our study and to go further than the surrounding, we now consider the spatial relation "*enlaced by*" in a more generic sense, in particular when the reference object has multiple degrees of concavities.

5.3.1. Illustrative example

Fig. 11 (a) presents a complex spatial configuration involving a spiral and different colored target

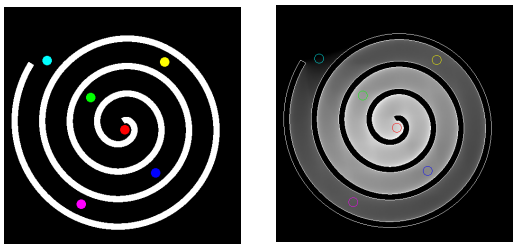

(a) (b) $\widetilde{\mu}_{\mathcal{E}}^{A}$

● (red)	[0.77, 0.89]
● (green)	[0.58, 0.63]
● (blue)	[0.53, 0.56]
● (yellow)	[0.33, 0.34]
● (purple)	[0.33, 0.35]
● (cyan)	[0.00, 0.08]

(c) Necessity-possibility intervals

Figure 11: Fuzzy enlacement landscape of a spiral (reference object A) and evaluation for different target objects inside the spiral (represented in different colors).

objects enclosed into it, from the center of the spiral to its "tail". The spiral is the reference object A, and we consider here its *Fuzz-DEL* $\widetilde{\mu}_{\mathcal{E}}^{A}$ that aggregates all directions. From this landscape (Fig. 11 (b)), we can observe the decreasing pattern (from white pixels to dark gray pixels) as we shift away from the center of the spiral. To assess this behavior, we measure the necessity-possibility scores between $\widetilde{\mu}_{\mathcal{E}}^{A}$ and each target object μ_B. Fig. 11 (c) presents the intervals $[N(\widetilde{\mu}_{\mathcal{E}}^{A}, \mu_B), \Pi(\widetilde{\mu}_{\mathcal{E}}^{A}, \mu_B)]$ measuring the global enlacement for the different target objects inside the spiral. Note that for this general enlacement experiment, we are not using the normalized projection of Equation 16, which was specifically introduced for the surrounding relation.

Note that other comparative approaches cannot take into account the depth within the spiral. For instance, the approach of Vanegas *et al.* [21], which was designed specifically to evaluate the surrounding relation, provides the same evaluations for the green, blue, yellow and pink objects (*i.e.*, around 0.50), because it does not consider the reference object as a whole, but only looks at the visible concavities from the boundaries of the target object.

5.3.2. Application to the MPEG7 shape dataset

In this experiment, we propose to apply our model to measure the quantity of enlacement that objects can exert around themselves. We considered the MPEG7 dataset[3], which is composed of 1400 images of binary shapes of various sizes, categorized into 73 different classes. This dataset is commonly used to benchmark shape classification methods [33]. Here, instead of considering classification, we use it to rank the object shapes according to their average quantity of enlacement, which can be considered as an appropriate measure of shape concavity and complexity.

We have first applied a pre-processing step to the dataset by: (1) applying a morphological closing to remove holes smaller than 1% of the object area, and then (2) removing shapes with more than one connected component since they are not particularly relevant for this experiment. Following this, we obtain a clean set of 1325 shapes with 71 classes.

For each shape A, we have computed the aggregated enlacement landscape $\widetilde{\mu}_{\mathcal{E}}^{A}$ (as in Fig. 11 (b) for example), obtained by averaging individual landscapes for a set of $k = 180$ linearly spaced $\theta \in [0, \pi]$. Then, we considered the average value in this aggregated landscape, summarizing into a single scalar value the quantity of enlacement exerted by the object, which we refer to as the *mean enlacement value*. Based on this framework, we decided to sort the different shapes of the dataset according to their respective mean enlacement values. We then simply normalized these ranking values into the $[0, 1]$ interval, such that the object with the maximum (resp. minimum) enlacement has a value of 1 (resp. 0). According to our model, objects with the highest rankings should correspond to concave shapes, as well as shapes exhibiting complex alternating patterns. In the same spirit, those with the lowest values should correspond to strictly convex shapes.

For comparison purposes, we applied a similar ranking framework with the recently proposed Q-concavity approach [30]. This method relies on counting the number of background pixels in each of the four quadrants for every point in the image, which can be efficiently computed using integral images and appropriate flips. From these counts, an average concavity degree is computed using appropriate normalization. In the same way, we applied a normalized ranking into $[0, 1]$ according to the Q-concavity evaluations, and we sorted the objects of the dataset from the highest to the lowest.

The results of this experiment can be observed in Fig. 12 and Fig. 13. On the one hand, Fig. 12

[3] `http://www.dabi.temple.edu/~shape/MPEG7/dataset.html`

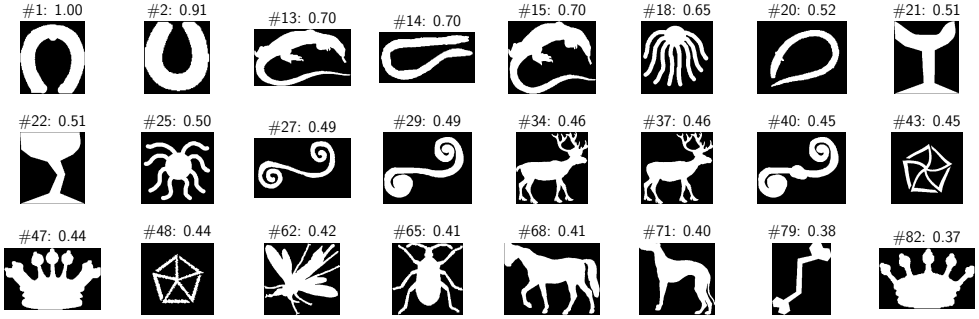

(a) 24 of the top ranked shapes according to our enlacement model

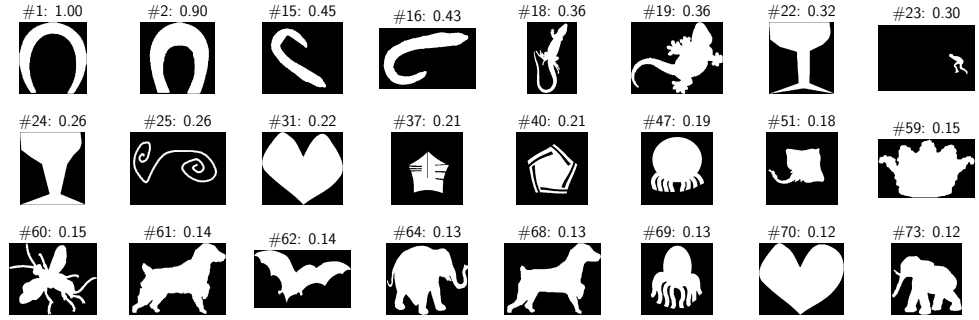

(b) 24 of the top ranked shapes according to the Q-concavity approach [30]

Figure 12: 24 of the top ranked shapes from the MPEG7 dataset (from left to right and top to bottom, limited to the top 2 shapes per class for better visualization) according to the normalized ranking values obtained from (a) our fuzzy enlacement landscape model, and (b) the Q-concavity approach proposed by [30].

shows the top 24 shapes with the highest normalized values for (a) our enlacement model and (b) the Q-concavity approach [30]. Notice how our enlacement model (a) allows to find concave patterns such as U-shape objects, but also more complex enlacement configurations such as spirals, tentacles or spiky extremities. While the comparative approach (b) also has concave shapes in the highest rankings, it seems to be less capable of finding more complex patterns with multiple levels of depths.

On the other hand, Fig. 13 shows the 24 shapes with the lowest normalized rankings. As expected, our approach only returns strictly convex shapes. However, the Q-concavity approach still finds objects with thin cavities (ranks #14 or #31 for example), as well as "T-shapes" (ranks #43 or #44) that are not convex. This might be due to the fact that this approach only considers a global information based on quadrants, and does not include directional information. Note that more specific results could be obtained for our approach according the the application requirement (*i.e.*, focus on a specific direction for example), while it is not possible with the approach of [30].

As an additional experiment, Fig. 14 shows the normalized ranking values for each shape of the dataset, sorted in a decreasing order (*i.e.*, left part of the curves correspond to shapes of Fig. 12, right part to shapes of Fig. 13). From this graph, we can observe a smoother decreasing profile for our proposed enlacement model, compared to the steep decreasing values obtained with the comparative Q-concavity approach. This result shows that our approach seems better suited to distinguish a wide variety of shape patterns, from very high complexity to more simple, strictly convex shapes. This could be useful in many pattern recognition applications.

5.4. Towards Fuzzy Interlacement Landscapes

Here, we also propose some preliminary results on the idea of *interlacement* landscapes. The term interlacement is intended as a mutual enlacement of two objects. If we aggregate all directions, a fuzzy interlacement landscape between two objects A and B can be obtained by: $\widetilde{\mu}_{\mathcal{I}}^{AB} = \widetilde{\mu}_{\mathcal{E}}^{A} + \widetilde{\mu}_{\mathcal{E}}^{B}$.

Fig. 15 shows the fuzzy interlacement landscapes obtained for several illustrative images, which have been respectively segmented into two objects (with

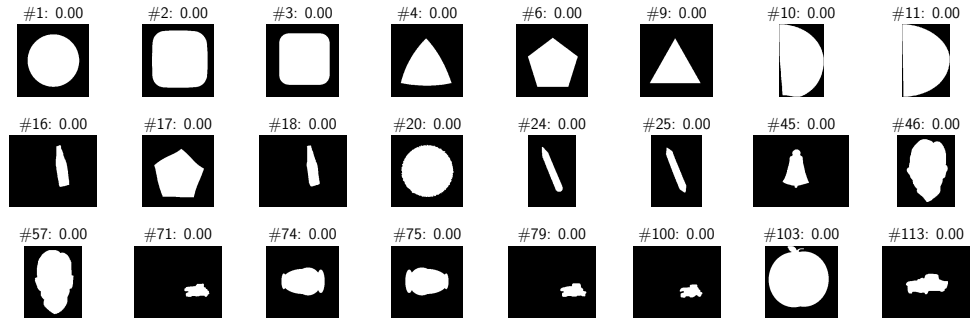

(a) 24 of the bottom ranked shapes according to our enlacement model

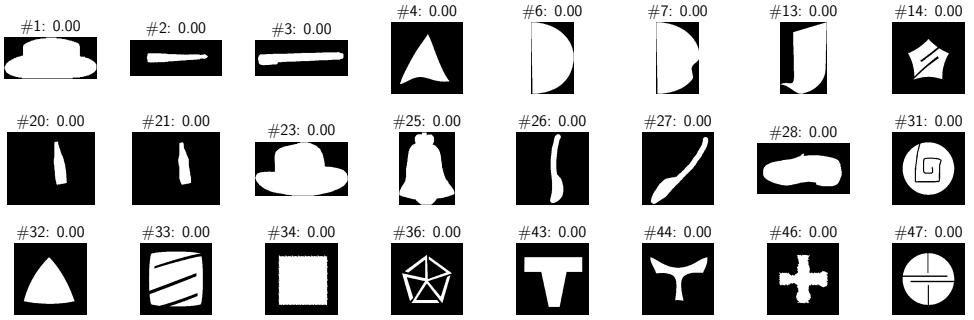

(b) 24 of the bottom ranked shapes according to the Q-concavity approach [30]

Figure 13: 24 of the bottom ranked shapes in the MPEG7 dataset (from left to right and top to bottom, limited to the bottom 2 shapes per class for better visualization) according to the normalized ranking values obtained from (a) our fuzzy enlacement landscape model, and (b) the Q-concavity approach proposed by [30].

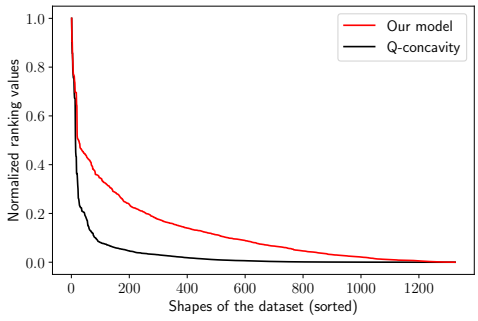

Figure 14: Sorted ranking values of the shapes of the MPEG7 dataset, for our fuzzy enlacement model and the Q-concavity approach of [30].

background in gray when applicable). The first landscape is obtained from an image of a zebra whose coat features an alternating stripes pattern. We can observe the high interlacement values concentrated in the center of the animal's coat. We can make the same kind of observation for wing patterns of the butterfly on the second example. The third landscape is obtained from an ASTER satellite image[4] covering a large delta river. Note that the interlacement is mainly located around the ramifications between the river and the mangrove. Such interlacement visualization could be useful, for instance, for ecological landscape monitoring. Finally, the last image is a decorative drop cap issued from an historical document, which has been binarized with a basic Otsu thresholding (therefore there is no background for this image). We can notice the stronger interlacement as we reach the center of the letter. We intend to exploit this visualization strategy more thoroughly in further works.

6. Conclusion

We introduced a generic fuzzy model for the evaluation of complex spatial configurations of binary objects represented in images. In particular, we focused on the enlacement relation, which generalizes the notion of surrounding, by taking into account object thickness and multiple components. Based

[4] U.S./Japan ASTER Science Team, NASA/GSFC/METI/ERSDAC/JAROS.

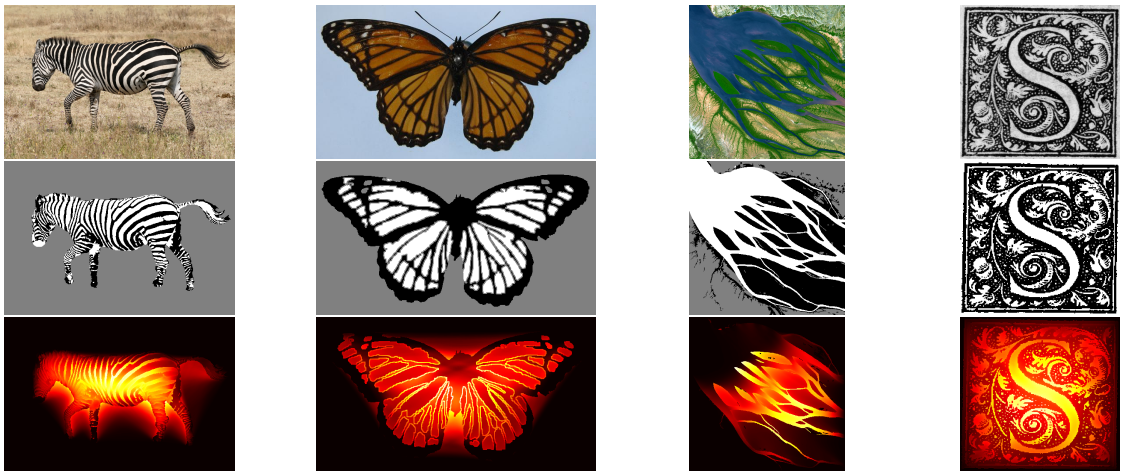

(a) Zebra (b) Butterfly (c) Delta river (d) Drop cap letter

Figure 15: Examples of fuzzy interlacement landscapes. The top line corresponds to the initial images, the second line shows the respective segmentations of the objects (white: object A; black: object B), and the third line shows the interlacement landscapes as heatmaps.

on the enlacement model [3], we proposed fuzzy enlacement landscape to assess this relation from a local point of view, taking into account the concavities of the objects in a directional fashion. We also put an emphasis on the invariance properties of these landscapes, such as translations, rotations and homotheties, which are often required in many pattern recognition tasks.

An experimental study carried out on different illustrative examples highlighted the interest of this model to evaluate the surrounding relation for various objects, and also to rank a wide variety of shape patterns, from high complexity to more simple, convex shapes. Furthermore, the behavior of our proposed fuzzy enlacement landscapes regarding to different types of transformations and alterations (rotations, scaling, noise) was studied, showing interesting properties that confirm our theoretical model.

In terms of limitations, our model could potentially suffer from some discontinuity issues, notably for example in the case of noise when pixels can be added outside of the reference object. To prevent this, we plan to design a more appropriate normalization strategy, also relying on the bandwidth parameter ω, or by considering non-standard discrete representations. This will be studied in future works. We also plan to further study how to exploit fuzzy interlacement landscapes, in particular with overlapping objects. Finally, our goal is to extend the model by integrating a measure of spacing in interlacement configurations, allowing to better take into account the distance between the objects.

Acknowledgement

This work was partially supported by the French *Agence Nationale de la Recherche* under Grant ANR-17-CE23-0015.

References

[1] J. Freeman, The Modelling of Spatial Relations, Computer Graphics and Image Processing 4 (2) (1975) 156–171.

[2] I. Bloch, Fuzzy spatial relationships for image processing and interpretation: A review, Image and Vision Computing 23 (2) (2005) 89–110.

[3] M. Clément, A. Poulenard, C. Kurtz, L. Wendling, Directional Enlacement Histograms for the Description of Complex Spatial Configurations between Objects, IEEE Transactions on Pattern Analysis and Machine Intelligence 39 (12) (2017) 2366–2380.

[4] M. Clément, C. Kurtz, L. Wendling, Fuzzy directional enlacement landscapes, in: Int. Conf. on Discrete Geometry for Computer Imagery (DGCI), 2017, pp. 171–182.

[5] I. Bloch, Fuzzy Relative Position between Objects in Image Processing: A Morphological Approach, IEEE Transactions on Pattern Analysis and Machine Intelligence 21 (7) (1999) 657–664.

[6] P. Matsakis, L. Wendling, J. Ni, A General Approach to the Fuzzy Modeling of Spatial Relationships, in: Methods for Handling Imperfect Spatial Information, 2010, pp. 49–74.

[7] D. Dubois, H. Prade, C. Testemale, Weighted fuzzy pattern matching, Fuzzy sets and systems 28 (3) (1988) 313–331.

[8] R. M. Cesar, E. Bengoetxea, I. Bloch, Inexact graph matching using stochastic optimization techniques for facial feature recognition, in: Int. Conf. on Pattern Recognition (ICPR), Vol. 2, 2002, pp. 465–468.
[9] O. Colliot, O. Camara, I. Bloch, Integration of fuzzy spatial relations in deformable models - Application to brain MRI segmentation, Pattern Recognition 39 (8) (2006) 1401–1414.
[10] A. Delaye, E. Anquetil, Learning of fuzzy spatial relations between handwritten patterns, International Journal on Data Mining, Modelling and Management 6 (2) (2014) 127–147.
[11] K. Miyajima, A. Ralescu, Spatial organization in 2D segmented images: Representation and recognition of primitive spatial relations, Fuzzy Sets and Systems 65 (2) (1994) 225–236.
[12] P. Matsakis, L. Wendling, A New Way to Represent the Relative Position between Areal Objects, IEEE Transactions on Pattern Analysis and Machine Intelligence 21 (7) (1999) 634–643.
[13] P. Matsakis, J. M. Keller, O. Sjahputera, J. Marjamaa, The use of force histograms for affine-invariant relative position description, IEEE Transactions on Pattern Analysis and Machine Intelligence 26 (1) (2004) 1–18.
[14] J. Ni, P. Matsakis, An equivalent definition of the histogram of forces: Theoretical and algorithmic implications, Pattern Recognition 43 (4) (2010) 1607–1617.
[15] P. Matsakis, J. M. Keller, L. Wendling, J. Marjamaa, O. Sjahputera, Linguistic description of relative positions in images, IEEE Transactions on Systems, Man, and Cybernetics, Part B: Cybernetics 31 (4) (2001) 573–88.
[16] A. R. Buck, J. M. Keller, M. Skubic, A memetic algorithm for matching spatial configurations with the histograms of forces, IEEE Transactions on Evolutionary Computation 17 (4) (2013) 588–604.
[17] S. Tabbone, L. Wendling, Color and grey level object retrieval using a 3D representation of force histogram, Image and Vision Computing 21 (6) (2003) 483–495.
[18] M. Clément, C. Kurtz, L. Wendling, Learning spatial relations and shapes for structural object description and scene recognition, Pattern Recognition 84 (2018) 197–210.
[19] I. Bloch, O. Colliot, R. M. Cesar, On the Ternary Spatial Relation "Between", IEEE Transactions on Systems, Man, and Cybernetics, Part B: Cybernetics 36 (2) (2006) 312–327.
[20] A. Rosenfeld, R. Klette, Degree of adjacency or surroundedness, Pattern Recognition 18 (2) (1985) 169–177.
[21] M. C. Vanegas, I. Bloch, J. Inglada, A fuzzy definition of the spatial relation "surround" - Application to complex shapes, in: European Society for Fuzzy Logic and Technology (EUSFLAT), 2011, pp. 844–851.
[22] P. Matsakis, S. Andréfouët, The fuzzy line between among and surround, in: IEEE Int. Conf. on Fuzzy Systems (FUZZ-IEEE), Vol. 2, 2002, pp. 1596–1601.
[23] N. Loménie, D. Racoceanu, Point set morphological filtering and semantic spatial configuration modeling: Application to microscopic image and bio-structure analysis, Pattern Recognition 45 (8) (2012) 2894–2911.
[24] C. M. Takemura, R. M. Cesar, I. Bloch, Modeling and measuring the spatial relation along: Regions, contours and fuzzy sets, Pattern Recognition 45 (2) (2012) 757–766.
[25] M. C. Vanegas, I. Bloch, J. Inglada, Alignment and parallelism for the description of high-resolution remote sensing images, IEEE Transactions on Geoscience and Remote Sensing 51 (6) (2013) 3542–3557.
[26] P. Matsakis, M. Naeem, F. Rahbarnia, Introducing the Φ-Descriptor – A Most Versatile Relative Position Descriptor, in: Int. Conf. on Pattern Recognition Applications and Methods (ICPRAM), 2015, pp. 87–98.
[27] P. Matsakis, M. Naeem, Fuzzy Models of Topological Relationships Based on the PHI-Descriptor, in: IEEE Int. Conf. on Fuzzy Systems (FUZZ-IEEE), 2016, pp. 1096–1104.
[28] J. F. Allen, Maintaining knowledge about temporal intervals, Communications of the ACM 26 (11) (1983) 832–843.
[29] M. Clément, M. Coustaty, C. Kurtz, L. Wendling, Local enlacement histograms for historical drop caps style recognition, in: IAPR Int. Conf. on Document Analysis and Recognition (ICDAR), 2017, pp. 299–304.
[30] S. Brunetti, P. Balázs, P. Bodnár, J. Szűcs, A Spatial Convexity Descriptor for Object Enlacement, in: Int. Conf. on Discrete Geometry for Computer Imagery (DGCI), 2019, pp. 330–342.
[31] K. Pluta, P. Romon, Y. Kenmochi, N. Passat, Bijective Digitized Rigid Motions on Subsets of the Plane, Journal of Mathematical Imaging and Vision 59 (1) (2017) 84–105.
[32] B. Bouchon-Meunier, M. Rifqi, S. Bothorel, Towards general measures of comparison of objects, Fuzzy Sets and Systems 84 (2) (1996) 143 – 153.
[33] H. Ling, D. W. Jacobs, Shape classification using the inner-distance, IEEE Transactions on Pattern Analysis and Machine Intelligence 29 (2) (2007) 286–299.

Appendix A. Proofs of Geometrical Properties

We provide hereinafter the proofs of the mathematical properties of the proposed fuzzy enlacement landscapes with regards to some geometric transformations.

Proof 1 (Translation). *In the frame oriented in direction θ, the translation operator $T_{\mathbf{v}}$ by vector $\mathbf{v} = [v_\rho, v_t] \in \mathbb{R}^2$ can be written as:*

$$f^{(\theta,\rho)}_{T_{\mathbf{v}}(A)}(t) = f^{(\theta,\rho-v_\rho)}_{A}(t - v_t). \tag{A.1}$$

Therefore, for any $(\rho, t) \in \mathbb{R}^2$, we have:

$$\mathcal{E}_{T_{\mathbf{v}}(A)}(\theta)(\rho, t) \tag{A.2}$$

$$= \frac{1}{\|T_{\mathbf{v}}(A)\|_1} \int_{-\infty}^{t} f^{(\theta,\rho)}_{T_{\mathbf{v}}(A)}(x)\,\mathrm{d}x \int_{t}^{+\infty} f^{(\theta,\rho)}_{T_{\mathbf{v}}(A)}(x)\,\mathrm{d}x \tag{A.3}$$

$$= \frac{1}{\|A\|_1} \int_{-\infty}^{t-v_t} f^{(\theta,\rho-v_\rho)}_{A}(x)\,\mathrm{d}x \int_{t-v_t}^{+\infty} f^{(\theta,\rho-v_\rho)}_{A}(x)\,\mathrm{d}x \tag{A.4}$$

$$= \mathcal{E}_A(\theta)(\rho - v_\rho, t - v_t) \tag{A.5}$$

It follows that $\mu_{\mathcal{E}}^{T_{\mathbf{v}}(A)}(\theta)(\rho,t) = \mu_{\mathcal{E}}^{A}(\theta)(\rho - v_\rho, t - v_t)$. □

Proof 2 (Rotation). *In the frame oriented in direction* θ*, the rotation operator* R_α *by angle* $\alpha \in \mathbb{R}$ *can be written as:*

$$f_{R_\alpha(A)}^{(\theta,\rho)}(t) = f_A^{(\theta-\alpha,\rho)}(t). \tag{A.6}$$

Therefore, for any $(\rho, t) \in \mathbb{R}^2$*, we have:*

$$\mathcal{E}_{R_\alpha(A)}(\theta)(\rho,t) \tag{A.7}$$

$$= \frac{1}{\|R_\alpha(A)\|_1} \int_{-\infty}^{t} f_{R_\alpha(A)}^{(\theta,\rho)}(x)\,\mathrm{d}x \int_{t}^{+\infty} f_{R_\alpha(A)}^{(\theta,\rho)}(x)\,\mathrm{d}x \tag{A.8}$$

$$= \frac{1}{\|A\|_1} \int_{-\infty}^{t} f_A^{(\theta-\alpha,\rho)}(x)\,\mathrm{d}x \int_{t}^{+\infty} f_A^{(\theta-\alpha,\rho)}(x)\,\mathrm{d}x \tag{A.9}$$

$$= \mathcal{E}_A(\theta-\alpha)(\rho,t). \tag{A.10}$$

It follows that $\mu_{\mathcal{E}}^{R_\alpha(A)}(\theta)(\rho,t) = \mu_{\mathcal{E}}^{A}(\theta-\alpha)(\rho,t)$. □

Proof 3 (Periodicity). *By definition we have, for any* $\theta, t \in \mathbb{R}$*,*

$$f_A^{(\theta+\pi,\rho)}(t) = f^{(\theta,-\rho)}(-t). \tag{A.11}$$

Hence, we have:

$$\mathcal{E}_A(\theta+\pi)(\rho,t) \tag{A.12}$$

$$= \int_{-\infty}^{t} f_A^{(\theta+\pi,\rho)}(x)\,\mathrm{d}x \int_{t}^{+\infty} f_A^{(\theta+\pi,\rho)}(x)\,\mathrm{d}x \tag{A.13}$$

$$= \int_{-\infty}^{t} f_A^{(\theta,-\rho)}(-x)\,\mathrm{d}x \int_{t}^{+\infty} f_A^{(\theta,-\rho)}(-x)\,\mathrm{d}x \tag{A.14}$$

$$= \int_{t}^{+\infty} f_A^{(\theta,\rho)}(x)\,\mathrm{d}x \int_{-\infty}^{t} f_A^{(\theta,\rho)}(x)\,\mathrm{d}x \tag{A.15}$$

$$= \mathcal{E}_A(\theta)(\rho,t). \tag{A.16}$$

It follows that $\mu_{\mathcal{E}}^{A}(\theta+\pi) = \mu_{\mathcal{E}}^{A}(\theta)$. □

Proof 4 (Scaling). *For* $\lambda \in \mathbb{R}$*, we have:*

$$\|S_\lambda(A)\|_1 = \lambda^2 \|A\|_1, \tag{A.17}$$

and:

$$f_{S_\lambda(A)}^{(\theta,\rho)}(t) = f_A(e^{i\theta}(\lambda t + i\lambda\rho)) \tag{A.18}$$

$$= f_A^{(\theta,\lambda\rho)}(\lambda t). \tag{A.19}$$

Therefore, using change of variable $y = \lambda x$*, we can write:*

$$\mathcal{E}_{S_\lambda(A)}(\theta)(\rho,t) \tag{A.20}$$

$$= \frac{1}{\|S_\lambda(A)\|_1} \int_{-\infty}^{t} f_{S_\lambda(A)}^{(\theta,\rho)}(x)\,\mathrm{d}x \int_{t}^{+\infty} f_{S_\lambda(A)}^{(\theta,\rho)}(x)\,\mathrm{d}x \tag{A.21}$$

$$= \frac{1}{\lambda^2\|A\|_1} \int_{-\infty}^{t} f_A^{(\theta,\lambda\rho)}(\lambda x)\,\mathrm{d}x \int_{t}^{+\infty} f_A^{(\theta,\lambda\rho)}(\lambda x)\,\mathrm{d}x \tag{A.22}$$

$$\underset{y=\lambda x}{=} \frac{\lambda^2}{\lambda^2\|A\|_1} \int_{-\infty}^{\lambda t} f_A^{(\theta,\lambda\rho)}(y)\,\mathrm{d}y \int_{\lambda t}^{+\infty} f_A^{(\theta,\lambda\rho)}(y)\,\mathrm{d}y \tag{A.23}$$

$$= \mathcal{E}_A(\theta)(\lambda\rho,\lambda t). \tag{A.24}$$

It follows that $\mu_{\mathcal{E}}^{S_\lambda(A)}(\theta)(\rho,t) = \mu_{\mathcal{E}}^{A}(\theta)(\lambda\rho,\lambda t)$. □